Experimental study of the stability and optimization of multipulse passive mode locking

Michael Katz,[1] Vladimir Smulakovsky,[1] Alexander Bekker,[1] Omri Gat,[2] and Baruch Fischer[1,*]

[1]*Department of Electrical Engineering, Technion, Haifa 32000, Israel*

[2]*Racah Institute of Physics, Hebrew University, Jerusalem 91904, Israel*

**Corresponding author: fischer@ee.technion.ac.il*

Received July 20, 2010; revised October 4, 2010; accepted October 6, 2010;
posted November 2, 2010 (Doc. ID 131826); published November 29, 2010

We present an experimental study of the stability of passively mode-locked pulses against noise in multipulse operation of an erbium-doped fiber laser. The laser properties are determined by two dimensionless combinations of the laser parameters. Measurements of the pulses' destabilization threshold as a function of those laser parameters show the optimal regions that maximize the mode-locked pulse stability. We find good agreement between the experimental observations and the theoretical predictions.

OCIS codes: 140.3430, 140.4050.

Passive mode-locking provides, in many cases, a cascaded abrupt formation of pulses as the laser pumping power increases [1,2]. Several recent theoretical and experimental studies have analyzed the mechanisms of multipulse formation and addressed the role of different mode-locked laser parameters [3–7]. The present work adds to the efforts of characterization of the mode-locked laser stability by taking into account the effect of laser noise, within the framework of the novel statistical light-mode dynamics (SLD) approach, which employs the tools of statistical mechanics to analyze multimode laser phenomena [8–15]. The SLD analysis of multipulse passive mode-locking [14] was based on rigorous mean-field calculations in the course-grained model [9]. It was theoretically and experimentally shown that a multi-pulse mode-locked laser is a thermodynamic-like system, with the role of temperature assumed by the intracavity noise, and with thermodynamic-like phases differing by the number of intracavity pulses. The phases are separated by first-order phase transition curves in the T–P plane (where P is the total intracavity power and T is the noise power), corresponding to the observed abrupt formation and annihilation of pulses. It was shown [14] that, when many pulses exist in the cavity, the individual pulse power maintains an almost constant value, determined by the saturation shape of the absorber transmissivity, and the phase transition curves are approximately equally spaced straight lines. The experimental work that verified the SLD theory [12,13] was done in a qualitative manner. While showing the basic phase transition behavior, it did not include direct quantitative dependence on the basic laser parameters: dispersion, gain filtering, saturable absorption, and the Kerr effect, which are not readily measured and controlled.

In the present work, we experimentally study the dependence of the pulse stability on the laser parameters. The theory is compared with experimental measurements in a fiber laser, passively mode locked by the nonlinear polarization rotation (NLPR) technique. Our main theoretical result is summarized in Eq. (3), which describes the phase transition line with n pulses. It follows that the phase transition line slope, which gauges the stability of mode locking against noise, depends on two dimensionless parameters. Experimentally controlling these parameters, we measured the pulse annihilation cascade and obtained the experimental values of the slopes. The experimental results are shown in Fig. 2 (below) and are compared with the theoretical predictions. As explained below, the limited accuracy of the measurement amounts to a single free parameter, which was fit simultaneously for all three curves. The results exhibit good quantitative agreement between theory and experiment over most of the parameter space; in particular, the curve maxima that correspond to the optimal parameter choice for pulse stability agree in theory and experiment.

The theoretical analysis is based on the Haus master equation model (the notations and the correspondence to [16] are discussed in [8,10]):

$$\dot{\psi} = (\gamma_g + j\gamma_d)\frac{\partial^2\psi}{\partial z^2} + [j\gamma_k|\psi|^2 + s(|\psi|^2) + g]\psi + \Gamma. \quad (1)$$

The coefficients γ_g, γ_d, and γ_k model the parabolic spectral gain filtering, chromatic dispersion, and Kerr nonlinearity, respectively. $s(|\psi|^2)$ is the transmissivity of the saturable absorber that describes the effective action of the NLPR [17]. Assuming that the mode locking is achieved for the optimal selection of the NLPR parameters (i.e., the polarization angles) it follows from Eq. (6) in [17] that $|s(|\psi|^2)|^2 = \frac{1}{2}\tau_R^{-1}[\sin(\tau_R\tilde{\gamma}_k|\psi|^2/(6\sqrt{2}))]^2$, where τ_R is the round-trip time. Here, $\tilde{\gamma}_k$ is the effective mean Kerr coefficient experienced by the waveform in NLPR, and, as discussed below, it is possible to decouple this parameter from the total intracavity Kerr coefficient γ_k. Note that, in the weakly saturated absorber limit, the transmissivity is [16,18] $s(|\psi|^2) = \gamma_s|\psi|^2$ with $\gamma_s = \tilde{\gamma}_k/12$. The cavity noise Γ is modeled as a white Gaussian noise with the autocorrelation function $\langle\Gamma^*(z',t')\Gamma(z,t)\rangle = 2LT\delta(z-z')\delta(t'-t)$, where T is the noise power injection rate per mode and L is the cavity length.

We study Eq. (1) via the gain balance method, previously employed in the limit of a weakly saturated absorber, where it was connected to the rigorous analysis of SLD [18]. The laser waveform is described as a combination of two parts—the short and strong pulses and the broad and weak noise-generated continuum. Then, for an n-pulse steady state, the total waveform

is written as $\psi = \sum_i^n \psi_{p(i)} + \psi_c$. We assume that the gain is saturated on a time scale much slower than the round trip, stabilizing the total intracavity power (energy over the round trip) to a constant value $\frac{1}{L}\int_0^L |\psi|^2 \mathrm{d}z = P$. This power is divided between the pulses, each carrying a fraction x_i of the total power P, and the continuum, carrying the remaining power fraction of $1 - \sum_i x_i$. Their dynamics is coupled via the amplifier gain, and the power distribution is established by imposing an identical gain on each of the waveform parts, due to the slow gain time scale. As in [13,14], in the following analysis we make a simplifying assumption that the pulses are noninteracting, i.e., are sufficiently spaced, and that they are of equal power so that $x_i = x$ and $\sum_i x_i = nx$.

The dynamics of the pulse waveforms is approximated by the noiseless version of the master equation [Eq. (1)]. Guided by experimental values, we make an assumption that the imaginary terms in Eq. (1) dominate the real terms, that is, we study the regime of solitonic pulse shaping. Then, the steady state of the individual pulse waveform is as follows [16,18]: $\psi_{p(i)} = A\,\mathrm{sech}(x(z - z_i)/l_p)\exp(j(\phi t + \varphi_i))$, where $A = x(PL/2l_p)^{1/2}$, $l_p = 4\gamma_d/\gamma_k LP$, $\phi = \gamma_k A^2/2$, and z_i and φ_i are the pulse position and phase shift, respectively. The pulse power dynamics is obtained by multiplying both sides of the noiseless equation by ψ_p^* and integrating with respect to z, which yields, in steady state, the relation

$$g(y) = \frac{\sqrt{2}}{4}\int_{-\infty}^{\infty}\left|\sin\left(\frac{y^2}{6\sqrt{2}}\mathrm{sech}^2(z')\right)\right|\mathrm{sech}^2(z')\mathrm{d}z' - \frac{y^2}{6}\frac{\gamma_k\gamma_g}{\tilde{\gamma}_k\gamma_d}, \tag{2}$$

where the integration limits have been extended to infinity since $L \gg l_p$, and we define the normalized pulse amplitude: $y = \sqrt{\tilde{\gamma}_k}A$.

The continuum waveform has a much weaker amplitude; therefore, the nonlinear term in Eq. (1) does not contribute significantly to its dynamics, determined by the linear terms and the noise source [18]. The continuum power in steady state as a function of the overall net gain has been calculated in [18], and it leads, according to the gain balance, to the relation

$$(1 - nx) = \frac{LT}{2P\sqrt{\gamma_g g(y)}}, \tag{3}$$

with $g(y)$ given by Eq. (2).

It was shown in [13,14] that the pulse power in multipulse mode locking remains close to a constant value $x = x_*$ that satisfies the implicit relation $G(y_*) = y_* g(y_*)$, where $G(y) = \int_0^y g(y')\mathrm{d}y'$. Then, in the case $n \gg 1$, the number of pulses in the steady state is the solution of Eq. (3) with $x = x_*$, $y = y_*$, rounded to the nearest integer. It follows that the phase transition curves are straight lines in the T–P plane (see Fig. 1), whose slope is $\frac{2}{L}\sqrt{\gamma_g g(y^*)}$. The slope value T/P can be rendered dimensionless by multiplying it by $L/\sqrt{\gamma_d}$, which then becomes a function of the two dimensionless parameters —$\tilde{\gamma}_k/\gamma_k$ and γ_d/γ_g; the numerically calculated dimensionless slope $2\sqrt{g(y^*)\gamma_g/\gamma_d}$ is shown in solid curves in Fig. 2.

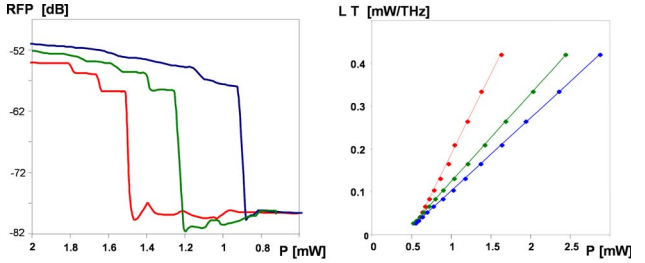

(a) (b)

Fig. 1. (Color online) (a) Pulse annihilation cascade—rf power versus optical power P, for three injected noise power levels LT (decreasing from left to right). (b) Injected noise power density LT as a function of the power P at the pulse destabilization threshold; measured data and fit lines for three values of spectral filtering width γ_g. Steeper slope corresponds to a higher pulse stability against noise. [The apparent crossing of the three lines is coincidental. The color scheme is coincidental and does not imply color correspondence between (a) and (b)].

The experiment was performed in a fiber-cavity NLPR mode-locked laser, with an Er-doped active fiber serving as the gain medium and an external amplified spontaneous emission (ASE) source providing injected noise power [13]. The NLPR method is based on the nonlinear fiber birefringence and the transmissivity of the polarization-controller–polarizer system is fixed by the nonlinear phase accumulation determined by the Kerr effect [17]. However, we show here that this constraint can be removed by replacing a section of the normal cavity fiber directly following the polarizer by a polarization maintaining (PM) fiber. Then, a pulse propagating in that section accumulates Kerr phase but does not experience NLPR. Thus, it is possible to achieve different values of $\tilde{\gamma}_k/\gamma_k$ ratio, between 1 (all-non-PM cavity) and 0 (all-PM cavity). Another directly controlled parameter is the spectral filtering coefficient γ_g. It was changed by means of an intracavity variable spectral filter—Santec OTF-350, manually tunable from 1 to 10 nm spectral width—inserted before

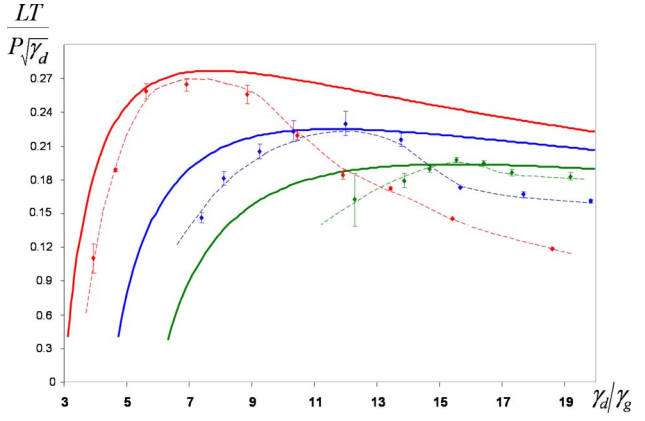

Fig. 2. (Color online) Theoretically calculated curves (solid) and the experimental observations of the dimensionless slopes $LT/P\sqrt{\gamma_d}$ of the pulse annihilation transition lines as a function of γ_d/γ_g, for three values of $\tilde{\gamma}_k/\gamma_k$: 1 (red, left), 2/3 (blue, middle), and 1/2 (green, right). The dashed curves are eye guides that connect the data points taken for a fixed value of $\tilde{\gamma}_k/\gamma_k$. The error bars show the accuracy of the linear fit on the data points shown in Fig. 1(b).

the gain fiber. Then, measurement of the total chromatic dispersion of the laser cavity completes the mapping of the system parameter space.

The pulse annihilation cascade for a constant level of injected noise power was measured by preparing the system in a many-pulse steady state, and gradually reducing the pumping power, while measuring both the out-coupled optical power and the rf power from a fast photodiode. The rf versus optical power for three different injected noise power levels are shown in Fig. 1(a), where the pulse annihilation events correspond to jumps in the rf power. We note that, as shown in [13,14], the mode-locked laser state is well described by the multipulse theory throughout the experimentally observed annihilation cascade, even though the solution of Eq. (3) is given for the case of highly multipulse operation. For different values of injected noise power, we measured the annihilation threshold of the last remaining pulse, which has the best measurement data quality. Figure 1(b) shows the resulting set of points and the corresponding linear fit, obtained for three different values of the filter's spectral width.

The dataset of the destabilization slope dependence on γ_g was measured in three cavity configurations, corresponding to three values of the parameter $\tilde{\gamma}_k/\gamma_k$: 1, $2/3$, and $1/2$. The obtained data is displayed in Fig. 2 with dashed guiding lines connecting points with a fixed $\tilde{\gamma}_k/\gamma_k$ value. Note that the intracavity power P cannot be directly measured but is estimated from the output power. Since the constant power model is approximate and the power fluctuates with the cavity elements, we estimate that the cavity power to output power ratio is double for the configurations containing the PM fiber due to additional coupling losses; this factor is taken into account in the data points shown in Fig. 2. There is also uncertainty in the injected noise power spectral density LT that is equal to the measured total noise power divided by the effective spectral width of the ASE source. The result is an order 1 factor of error in the experimental value of LT/P that we used as a fitting parameter in comparison with the theoretical predictions. The best fit was obtained when this factor was approximately $3/2$, and the comparison is shown in Fig. 2. Evidently, there is a good quantitative agreement between experiment and theory for a wide range of laser parameters, particularly in the correspondence of the maxima of the theoretical and experimental curves—a result independent of the fitting procedure. The likely cause of the discrepancy for the rest of the parameters lies in some of the simplifying assumptions made in the theoretical analysis, mainly the solitonic pulse shaping, and the use of results derived for many-pulse steady states beyond their strict domain of validity. These theoretical limitations can be removed by a straightforward extension of the present theory if the need for higher accuracy arises.

In conclusion, we have shown that the basic underlying physics of the pulse-formation–annihilation process in a passively mode-locked fiber laser is well described by the SLD theory, confirming that this theory can be used for prediction and design of mode-locked laser operation. We have identified two dimensionless parameters governing the light-mode dynamics in our experimental system and analyzed the phase diagram for a wide range of these parameters experimentally and theoretically with good correspondence. In particular, we have shown that, for certain parameter relations, the noise destabilization curves in Fig. 2 exhibit maximal values—optimizing the laser configuration to reach this parameter region will lead to the most stable mode-locked operation.

This research was supported by the Israel Science Foundation (ISF).

References

1. V. J. Matsas, D. J. Richardson, T. P. Newson, and D. N. Payne, Opt. Lett. **18**, 358 (1993).
2. D. Y. Tang, W. S. Man, and H. Y. Tam, Opt. Commun. **165**, 189 (1999).
3. V. L. Kalashnikov, E. Sorokin, and I. T. Sorokina, IEEE J. Quantum Electron. **39**, 323 (2003).
4. A. Komarov, H. Leblond, and F. Sanchez, Phys. Rev. A **71**, 053809 (2005).
5. B. G. Bale, K. Kieu, J. N. Kutz, and F. Wise, Opt. Express **17**, 23137 (2009).
6. X. Liu, Phys. Rev. A **81**, 023811 (2010).
7. F. Li, P. K. A. Wai, and J. N. Kutz, J. Opt. Soc. Am. B **27**, 2068 (2010).
8. A. Gordon and B. Fischer, Phys. Rev. Lett. **89**, 103901 (2002).
9. O. Gat, A. Gordon, and B. Fischer, Phys. Rev. E **70**, 046108 (2004).
10. O. Gat, A. Gordon, and B. Fischer, New J. Phys. **7**, 151 (2005).
11. R. Weill, A. Rosen, A. Gordon, O. Gat, and B. Fischer, Phys. Rev. Lett. **95**, 013903 (2005).
12. A. Gordon, B. Vodonos, V. Smulakovski, and B. Fischer, Opt. Express **11**, 3418 (2003).
13. B. Vodonos, R. Weill, A. Gordon, A. Bekker, V. Smulakovsky, O. Gat, and B. Fischer, Phys. Rev. Lett. **93**, 153901 (2004).
14. R. Weill, B. Vodonos, A. Gordon, O. Gat, and B. Fischer, Phys. Rev. E **76**, 031112 (2007).
15. A. Rosen, R. Weill, B. Levit, V. Smulakovsky, A. Bekker, and B. Fischer, Phys. Rev. Lett. **105**, 013905 (2010).
16. H. A. Haus, IEEE J. Sel. Top. Quantum Electron. **6**, 1173 (2000).
17. C.-J. Chen, P. K. A. Wai, and C. R. Menyuk, Opt. Lett. **17**, 417 (1992).
18. M. Katz, A. Gordon, O. Gat, and B. Fischer, Phys. Rev. Lett. **97**, 113902 (2006).